

OSL ages that inform late phases of dune formation and human occupation near Olympic Dam in northeastern South Australia

MARJORIE SULLIVAN, TRAEVIS L. FIELD, PHILIP HUGHES, BEN MARWICK
PAULINA PRZYSTUPA AND JAMES K. FEATHERS

Marjorie Sullivan, Philip Hughes: HEH Pty Ltd PO Box 97 Moruya NSW 2537 and RMAP The Australian National University, Canberra 0200 Email: heh@bigpond.net.au

Traevis L. Field, Ben Marwick, Paulina Przystupa, James K. Feathers:

Department of Anthropology, Box 353100, University of Washington, Seattle, WA. 98195-3100

Email: Traevis L. Field (tfield@uw.edu), Ben Marwick (bmarwick@uw.edu) Paulina Przystupa (ciszka@uw.edu)

James K. Feathers (jimf@uw.edu):

Abstract

The Olympic Dam archaeological salvage program covers an area of 600 km² and contains more than 16,500 archaeological sites, most of which are open scatters of stone artefacts on linear sand dunes. Optically stimulated luminescence (OSL) dating offers an opportunity to date recent phases of dune movement and stability, and to provide a chronology for archaeological material on and in the sand bodies.

Initial OSL ages from one large site in a deflation hollow on a dune are presented here. The dating was undertaken as part of a student project, and the results provide information on sand accumulation from about 12,000 years ago, with human occupation at the site occurring after that time.

Introduction and background

The ongoing Olympic Dam archaeological salvage program has been described by Hughes *et al.* (2011). It is a large research-oriented program following on from archaeological impact assessments at Olympic Dam in arid northeast South Australia (Figure 1).

In 1980 Hughes, Hiscock and colleagues commenced archaeological investigations for the Olympic Dam mining project (Figure 1). These continued as small area surveys, linear surveys for infrastructure corridors, and from 2007 to 2009 as a block survey of about 515 km² for the proposed expansion of the mine. In these investigations Hughes and Hiscock developed an environmentally-based predictive model (see Hughes *et al.* 2011) that used terrain pattern mapping based on a combination of landform types and underlying geology. Landform types were used to predict the location and frequency of occurrence of suitable 'campsites', sources of water and ease of movement across the landscape. Geology was used to predict the availability of different rock types for stone artefact manufacture. The model has proved to be robust, and has been used to underpin a survey strategy, and to locate, record and explain the distribution of more than 16,500 archaeological sites in the Olympic Dam area (Hughes *et al.* 2011). The sites were recorded using hand-held computers, and the survey records are consistent for the whole expansion area.

Almost all of the sites comprise surface scatters of flaked stone artefacts. Hearths, grindstones, ochre and manuports are found on some sites, and quarries and other procurement areas occur, but none of the sites recorded contain organic materials. Flaked stone artefacts form the basic materials for further analyses.

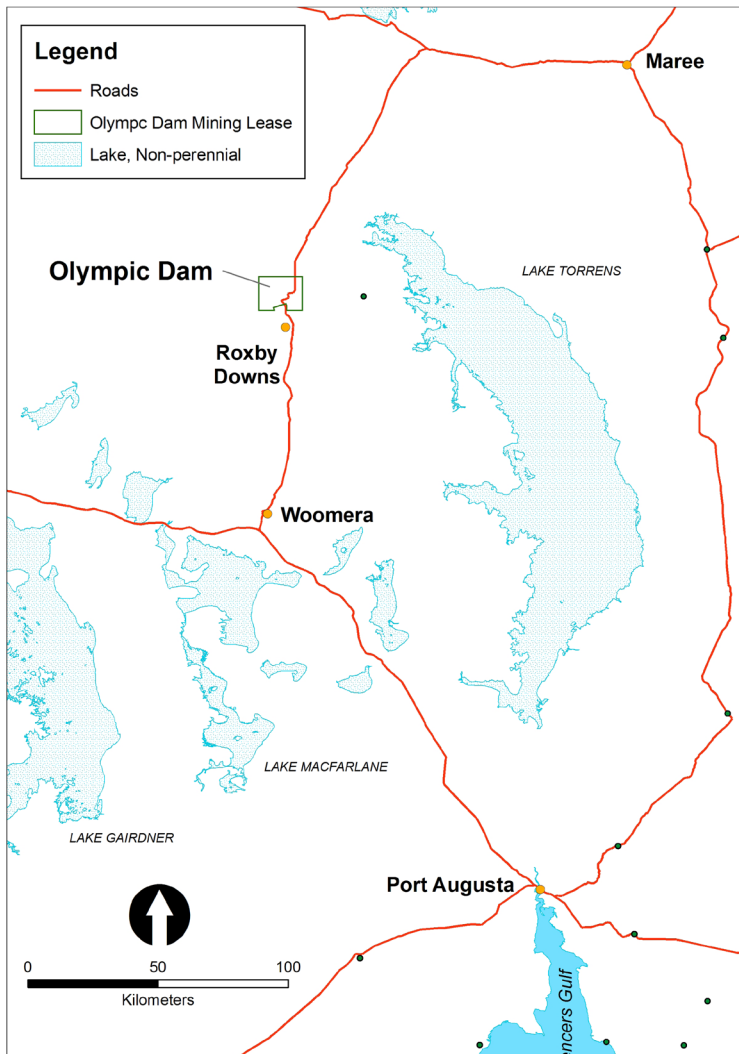


Figure 1. Location of the study area in South Australia. Map produced by BHP Billiton.

Following the survey phases, an archaeological salvage program commenced in mid-2010, and involved surface collection and excavation at 150 selected sites. In determining the number of sites and which sites warranted further study, several principles were employed as described in Hughes *et al.* (2011), which acknowledged that sites with high potential for scientific investigations are those with high chronological and spatial resolution.

Geoarchaeological questions at site ODO3A23 at Olympic Dam

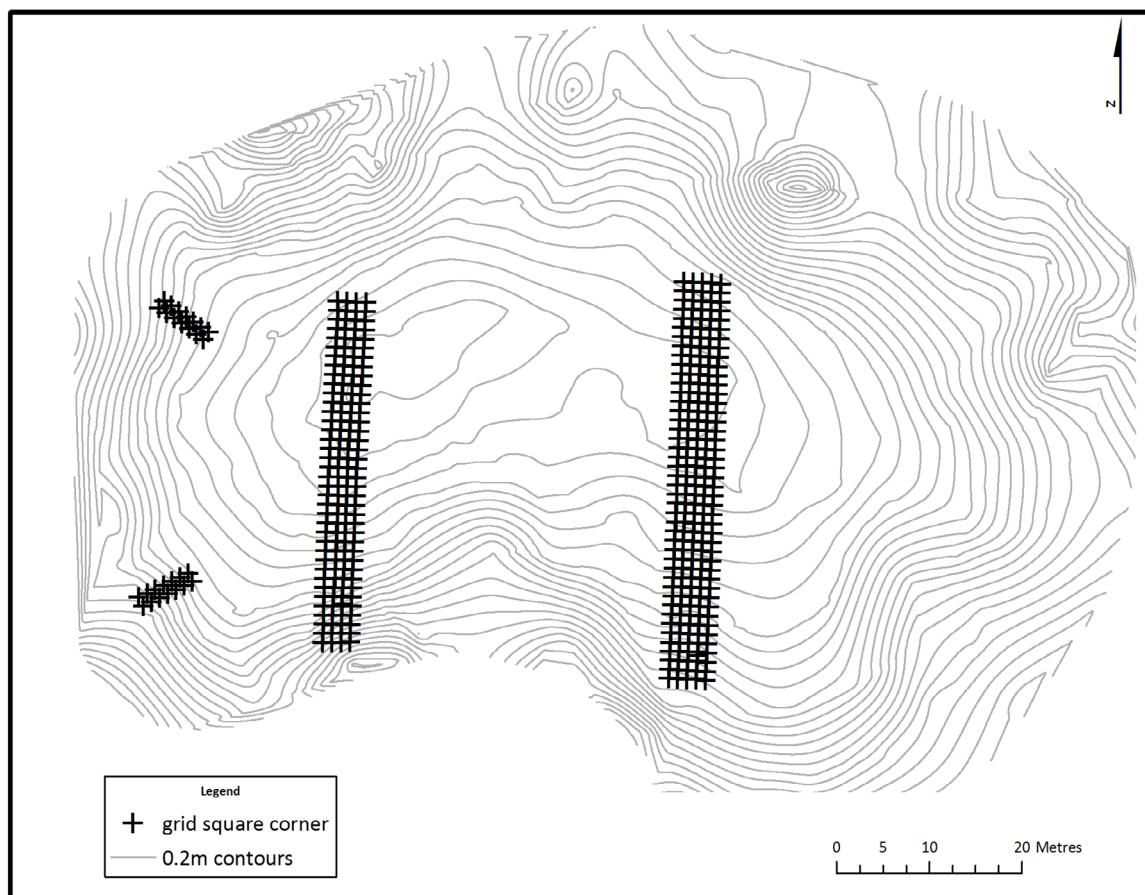
The salvage program based on the survey results and these principles commenced in July 2010. A University of Washington (UW) archaeological field school (under the direction of Dr Ben Marwick) was supported by the salvage program, and commenced in July 2010, very soon after the salvage program had begun. The field school students worked on some of the sites identified as having high priority, close to the mine and in areas that would be affected by the earliest stages of the proposed mine expansion. One site was a very large scatter of stone artefacts covering about 200 m² in a 2-5m deep wind-deflated depression (blowout) on a longitudinal sand dune immediately north of the existing mine - designated ODO3A23 (Figure 2).

This was a high priority site for salvage because of its location, and as it was considered to have potential to address some of the general questions posed for the Olympic Dam archaeological salvage program, including questions of occupational chronology:

- Did people who occupied the area in the past camp in existing blowouts which have retained their general form over long periods of time, or have the blowouts formed subsequently, with stone artefacts having being lowered as the deflation process occurred?
- Did an occupied blowout change its form after the main phase(s) of past occupation?
- Are there archaeological materials buried around the rims of blowouts? If so is their nature and content similar to the materials exposed in the blowout?
- Is it possible to date occupation of the blowout? Do any parts of the site show spatial or chronological integrity?
- Is it possible to date the age of the dune or the surface on which occupation occurred?

Sediment samples for OSL dating from ODO3A23 were analysed as a student project at the University of Washington Luminescence Dating Laboratory.

Figure 2. Site ODO3A23 showing the blowout, the two main artefact collection grids and the two excavated trenches on the western rim of the blowout. The OSL samples were taken from the southwestern wall of the northwestern-most square of the northern trench.



SAMPLE	UW2555	UW2556	UW2557	UW2558
Grains (n)	165	201	99	161
Burial Depth (mm)	395	495	645	845
D_E (Gy)	0.78 ± 0.19 *	5.85 ± 0.12	6.08 ± 0.18	5.94 ± 0.14
σ_b (%)	154 ± 20	22 ± 2	26 ± 2	23 ± 2
RADIOACTIVITY				
^{238}U (ppm)	0.55 ± 0.05	0.56 ± 0.05	0.33 ± 0.04	0.22 ± 0.04
^{232}Th (ppm)	0.88 ± 0.32	0.88 ± 0.33	1.42 ± 0.40	1.67 ± 0.48
^{40}K (%)	0.07 ± 0.01	0.10 ± 0.02	0.07 ± 0.02	0.08 ± 0.01
Dose Rates (Gy/ka)				
Alpha	0.16 ± 0.02	0.18 ± 0.02	0.14 ± 0.02	0.14 ± 0.02
Beta	0.19 ± 0.02	0.14 ± 0.02	0.19 ± 0.03	0.20 ± 0.02
Total D_R (Gy/ka)	0.46 ± 0.05	0.48 ± 0.05	0.44 ± 0.05	0.46 ± 0.05

Table 1. Radioactivity measurements, equivalent dose values and age determinations for site ODO3A23 samples. *The central age estimate of UW2555 was calculated from the 79 grains with a positive value. The others had a negative D_E value indicating modern sand, and were not analysed.

OSL as a dating method for inorganic sediments in arid Australia

Dating of sediments using optically stimulated luminescence (OSL) has become important for studying earth surface processes (e.g., Rhodes 2011). Luminescence methods estimate the time since individual grains of quartz and feldspar were last exposed to sunlight. The dating range extends from very recent deposits to sediments deposited hundreds of thousands of years ago.

Mabbutt (1977) argued that the longitudinal dunefields and the basal imprints of the dunes in arid Australia are ancient - dating from the early Pleistocene. OSL dating has been used subsequently to investigate the chronology of dune formation and the possible human use of those environments (Murray-Wallace *et al.* 2002, Magee *et al.* 2004, Hesse *et al.* 2004, Hollands *et al.* 2006, Twidale *et al.* 2007, Lomax *et al.* 2007, Fitzsimmons *et al.* 2007), and luminescence ages have provided information about more recent phases of sand movement on and along the upper sections of these dunes.

The ages show a general association between dune building and aridity. Phases of dune-building activity have been identified from the Lake Eyre region and from the Strzelecki and Tirari Deserts during cold dry periods between about 50 ka and 35 ka, and again at the end of the last glacial maximum, from about 23 ka to a period between 12 and 14.5 ka (Fitzsimmons *et al.* 2007). Dune-building activity diminished in the Strzelecki and Tirari Deserts from the late Pleistocene into the early Holocene (Fitzsimmons *et al.* 2007) and the Tasman Sea dust record includes a peak of aeolian deposition ending at around the same time suggesting this was a widespread phenomenon (Hesse 1994). After about 12 ka, as the climate became wetter in the early Holocene, increased vegetation cover reduced aeolian

activity (Hesse *et al.* 2004). There are suggestions from the dune records of the Tirari and Strzelecki Deserts (Fitzsimmons *et al.* 2007), from thermoluminescence ages from the Simpson Deserts (Nanson *et al.* 1992; 1995), and from pollen and OSL dates from the Darling Basin (Copper 2005), that dune stability was associated with wetter conditions in the early to mid-Holocene, and dune remobilisation with drier conditions in the late Holocene after about 5 ka.

Lack of preserved organic material prevents the use of radiocarbon to date these sites, so other chronometric methods must be used. At Olympic Dam only relative ages for the region's surface archaeology have so far been suggested. The presence of characteristic artefact types such as numerous backed artefacts, pirri points and tula adzes, whose contexts have been well-dated in other Australian regions, as well as the location of the assemblages on surfaces believed to be of post-Pleistocene deposition, suggest that most of the stone artefacts in surface scatters are relatively recent, dating to the mid/late Holocene (Hughes and Hiscock 2005, Mitchell, 2005).

Archaeological investigations at ODO3A23

Two 1 m grid square transects were placed through two surface artefact clusters at ODO3A23, one on the western and one on the eastern side of the blowout (Figure 2), each in a minor depression within the blowout. The total area from which artefacts were collected from the surface and the underlying 100mm of sand was 138 m². The artefact densities of this surface and near-surface scatter were 20/m² in the western transect and 27/m² in the eastern transect.

On the western margin of the blowout, stone artefacts appeared to have been buried by sand that had cascaded down its rim. The extension of an artefact layer from a blowout into the slumped/windblown sand on its margin is similar to the situation reported from another

site in a blowout at Olympic Dam (H364) by Mitchell (1985) who did not attempt to date the artefact layer within the dune.

In order to date this buried artefact layer, two 6 m X 1 m excavation areas were gridded on the western margin of the blowout (Figure 2). All surface artefacts and manuports were collected within the grid squares, and the sand deposits were excavated in horizontal 100 mm-deep spits and sieved to recover artefacts, to trace any artefact layer in its stratigraphic context and to obtain datable sediment samples. Excavations continued until culturally sterile sediments were reached at a maximum depth of 800mm.

In the southern trench, artefacts occurred only on the surface and in the top 50-100mm of loose sand. No OSL samples were collected from this trench.

In the northern trench an upper root-penetrated layer of red sand thickened upslope from about 50mm to 400mm. This upper sand retained visible thin near-horizontal aeolian bedding, suggesting it was very recent, as the sand had not yet been subject to appreciable bioturbation. Below 400 mm the deposit was undifferentiated loose red well-sorted medium quartz sand, and there was a sharp break between the bedded sand and the undifferentiated sand. Almost all the stone artefacts were recovered from the base of the bedded surface sands, concentrated in a layer at that break.

Sediment 'core' samples were collected for OSL dating from the northern trench using opaque PVC cylinders, 50 mm in diameter and 200 mm long. Three cylinders were inserted horizontally into the southwestern wall of the excavation trench (Figure 2), to sample the base of the bedded upper sediments (400 mm below surface), the sand immediately below that bedding (500 mm) and the undifferentiated sand near the base of the excavation (700 mm). A fourth core was inserted vertically into the excavation floor, about 1 m below the ground surface to obtain the earliest date that could be ascertained from this excavation (Table 1).

OSL sample preparation

Standard procedures for obtaining quartz grains were followed for the OSL determinations.

- Sample preparation was conducted under subdued indirect red lighting.
- Only the unexposed central material from the cylinders was used for luminescence measurements.
- Moisture content was determined from 100g voucher samples taken to provide a backup of material.
- The samples were dry-sieved mechanically through nested brass sieves into several grain size fractions. Only the 180-212µm grains were used for analysis as these fit into the 300µm holes in the single-grain disks.
- The grains were first treated with hydrochloric acid and hydrogen peroxide to remove carbonate and organic materials. No reaction was visible with either.

- A 40 minute hydrofluoric acid etch was employed to remove outer surfaces of the grains (which might be subject to external alpha radiation) and to reduce feldspars. The grains were treated again with HCl and then resieved to remove any remnant feldspars.
- A density separation using a metalithium-tungstate solution of 2.67 specific gravity) was used to remove heavy minerals.

Luminescence analysis

Luminescence dating relies on the principle that materials absorb energy from naturally occurring ionising radiation and release that energy, in part as luminescence, with exposure to light or heat (Aitken 1998). The intensity of the luminescence signal is proportional to the time since the last exposure. Dose rate (D_R), the denominator for the equation to calculate age, is the average radiation dose that a sample is exposed to over time. This includes alpha, beta, gamma and cosmic radiation, although for etched quartz grains the alpha contribution is negligible. The primary terrestrial sources of radiation are ^{40}K , ^{238}U , and ^{232}Th . The numerator in the age equation is the equivalent dose (D_E): the radiation dose necessary to produce a luminescence signal equal to the natural signal measured in the laboratory. The equation:

$$\text{Age(ka)} = D_E (\text{Gy}) / D_R (\text{Gy/ka})$$

is used to determine age in thousands of years (ka), D_E is measured in grays (the international unit for absorbed dose, in J/kg) and D_R is measured in grays per thousand years.

Grains were placed onto five discs (eight discs for U2556) for single-grain measurement. One disc from each sample was used to measure dose recovery, and the other four for equivalent dose.

Luminescence was measured on a Risø TL-DA-15 reader with single-grain attachment. Stimulation was by a 532 nm laser delivering 45 W/cm². Detection was through 7.5 mm U340 (ultraviolet) filters. Exposure was for 0.8 s on each grain at 125°C. The first 0.06 s was used for analysis and the last 0.15 s for background. A preheat of 240°C for 10 seconds followed each dose, except for the calibrating test doses after which a 200°C for 1 second preheat was employed. The test dose was about 3 Gy. Doses were delivered by a 90 Sr beta source which provides about 0.1 Gy per second to coarse-grained quartz.

Equivalent dose (D_E) was estimated using single aliquot regeneration (SAR) protocol on single grains (Murray and Wintle 2000, Wintle and Murray 2006). The SAR method which measures the natural signal and that from a series of regeneration doses, provides three benefits for D_E calculation (Murray and Wintle, 2000; Wintle and Murray 2006). It makes extrapolation of values to determine ages unnecessary, it includes a correction for sensitivity changes and it allows for samples containing mixed sediments to be identified. The method uses a small test dose to monitor and correct for sensitivity changes brought about by preheating, irradiation or light stimulation.

SAMPLE	DEPTH (mm)	COMPONENT 1		COMPONENT 2		COMPONENT 3		CENTRAL AGE MODEL (ka)
		De (Gy)	%	De (Gy)	%	De (Gy)	%	
UW2555	395	0.24±0.05	63.4	2.47±0.15	11.4	6.01±0.23	25.2	5.09 ± 0.68
UW2556	495	3.36±0.18	4.8	5.35±0.10	61.4	7.40±0.21	33.8	12.1 ± 1.28
UW2557	645	5.01±0.26	42.5	6.50±0.31	47.9	11.0±0.63	9.6	13.9 ± 1.59
UW2558	845	4.66±0.13	38.2	6.30±0.19	42.1	8.50±0.34	19.8	12.8 ± 1.40

Table 2. Components containing highest percentage of sample measurements and central age model for ODO3A23 samples.

Single-grain analysis also provides the opportunity to remove from analysis grains with unsuitable characteristics. Grains were eliminated if they had poor signals (errors on the test dose greater than 30% or from net natural signals not at least three times above the background standard deviation); did not produce within 20% the same (recycling) signal ratio from identical regeneration doses at the beginning and end of the SAR sequence; yielded natural signals that did not intersect saturating growth curves; had a signal larger than 10% of the natural signal after a zero dose; or contained feldspar contaminants (judged visually on growth curves by a reduced signal from infrared stimulation on two doses).

The luminescence signal from quartz has multiple components, some bleaching more rapidly than others. Linearly-modulated OSL (where the laser power is ramped from 0 to 90% in 30 seconds) allows visual separation of the components and identification of those grains dominated by other than the fast-bleaching component. This minimises the effect of partial bleaching, where sunlight is inadequate to reset the signal (Murray and Wintle 2000). Linearly-modulated OSL was measured for each grain at the end of each SAR sequence. Grains dominated by other than the fast component were marked, and if the D_e from these differed significantly from those of fast-component grains, they were removed from analysis.

A dose recovery test was performed on some grains. Their luminescence was removed by exposure to the laser, a dose of known magnitude administered and the SAR procedure was applied to see if the known dose could be obtained.

A D_e value was obtained for each suitable grain. Because of varying precision, a distribution is produced. Two statistical tools - the common age model and central age model (Galbraith *et al.* 1999, 2005) are used to evaluate D_e distributions. The common age model controls for differential precision by computing a weighted average using $\log D_e$ values. The central age model assumes a natural distribution of D_e values, because of non-statistical sources of variation, and computes an over-dispersion parameter (σ_b) as the

relative standard deviation (or coefficient of variance) of the true D_e values: deviation beyond that accounted for by measurement error. Empirical evidence suggests that σ_b of between 10 and 20% is typical of single-aged samples (Olley *et al.* 2004; Jacobs *et al.* 2006). For samples of mixed ages either a minimum age model or a finite mixture model is used. The minimum age calculates a statistical minimum using a truncated normal distribution and is suitable for partially bleached samples. The finite mixture model may be used if post-depositional processes have discrete age populations. It uses maximum likelihood to separate grains into single-aged components based on the input of a given σ_b value and the assumption of a log normal distribution of each component. The model estimates the number of components, the weighted average of each component, and the proportion of grains assigned to each. The model provides two statistics for estimating the most likely number of components, maximum log likelihood (l_{ik}) and Bayes Information Criterion (BIC).

Dose rate determinations

Radioactivity was measured by alpha counting, beta counting and, for K, atomic emission. Samples for alpha counting were crushed, packed into plexiglass containers with ZnS:Ag screens, and sealed for one month. The pairs technique was used to separate the U and Th decay series. For atomic emission measurements, samples were dissolved in hydrofluoric and other acids and analysed by a Jenway flame photometer. K concentrations for each sample were determined by bracketing between standards of known concentration. Conversion to ^{40}K was by natural atomic abundance. Radioactivity was measured by beta counting using a Risø low level beta GM multicounter system for 24 hours. The average was converted to dose rates following Bøtter-Jensen and Mejdahl (1988) and compared with the beta dose rate calculated from alpha counting and flame photometer results. Cosmic radiation was determined after Prescott and Hutton (1988) using site latitude, longitude and altitude. Radioactivity concentrations were translated into dose rates following Adamiec and Aitken (1998).

Age was calculated using a laboratory-constructed spreadsheet based on Aitken (1985). Error terms were computed at one-sigma. These measurements are detailed in Table 1.

Dosimetry results

The concentrations of the major radionuclides are given in Table 1, along with the total dose rate. Also given is the beta dose rate calculated in two ways: directly from beta counting and indirectly from alpha counting and flame photometry. These are in agreement for three samples. A small discrepancy for UW2558 may reflect some disequilibrium, but whatever the cause, beta counting, as a direct measure, is considered more accurate and was used for the beta dose rate in age calculation. Moisture content was taken to be $2 \pm 2\%$, which reflects the measured amount. The dose rates for all samples are low, reflecting a composition dominated by quartz. The low dose rates mean that the relative cosmic dose contribution is high, about 45%, increasing uncertainty.

Equivalent dose (D_E) was measured on single-grains using 180-212 μm quartz. About 500 grains were measured for each sample, with 700 measured for UW2556. These were all used for equivalent dose determination except for 100 grains from UW2556, which were used for dose recovery. The acceptance rate was relatively high: 41.2% for UW2555, 28.7% for UW2556, 19.8% for UW2557, and 32.2% for UW2558. A total of 42 grains from the 100 grains of UW2556 were acceptable for dose recovery. For the latter the administered dose was 40s of beta irradiation, and the central tendency of the recovered doses was $40.8 \pm 0.9\text{s}$, with an over-dispersion of 5.3%. This suggests that the procedures were working properly. The 5.3% over-dispersion is the minimum dispersion that might be expected for a single-aged sample, due to variations in luminescence from grain to grain, machine scatter, or other measurement variables. All extrinsic sources of over-dispersion – different depositional ages or differential dose rate – are controlled in dose recovery, so over-dispersions above about 5% in the natural D_E distributions can be attributed to these extrinsic factors.

The natural distributions are summarised in Table 1. This gives the number of grains for which a D_E could be derived, the central tendency expressed as the central age model, and the over-dispersion (σ_b (%)). Over-dispersion was not high for three of the samples, but it was higher than the 5% from dose recovery, so some extrinsic factors are involved. The over-dispersion for UW2555 is very high so a finite mixture model was applied, using 5% over-dispersion to account for intrinsic factors. The number of components derived is a function of extrinsic factors only. Table 2 gives for each sample the D_E value for each component as well as the proportion of grains assigned to each.

Some over-dispersion is due to differential dose rate. The D_E is measured on single grains but the dose rate used to determine age is the bulk value from the sample. The beta dose rate may vary at the scale

of single grains depending on the distribution of radioactive sources relative to the individual grains. For sandy sediments where potassium feldspars are sparse and unevenly distributed, grains close to them will have a higher ^{40}K dose rate than those further away. A simulated model (Mayya *et al.* 2006) was applied to determine a probable minimum dose rate for grains far from beta sources, based on the percentage of ^{40}K in the samples and the proportion of the total dose rate contributed by betas. (Long-range gamma radiation does not normally produce heterogeneous dose rates, and short-range alpha radiation is not significant for coarse-grained quartz.) The D_E value from the lowest component was divided by this minimum dose rate and the age compared with the age of the second component.

For UW2557 and UW2558, this procedure produced no significant difference in age between the first and second components, suggesting beta heterogeneity could account for the difference. This was not true for the second and third components, suggesting older grains were present, but the third component is relatively small and some of it may be accounted for by differential dose rate. Both samples are therefore close to being single-aged samples, and the central age model, which averages out differences in beta dose rates, is a good estimate for deriving the age of deposition.

For UW2556, beta heterogeneity cannot account for the difference between the first and second components. The first component is small and consists of grains derived from the sediments just above the sample. The difference between the second and third components, when accounting for differential beta dose rate, was low (not significant at two sigma), suggesting some mixing of older grains. This sample is nevertheless close to being single-aged, and the central age model provides the best estimate. The central age D_E values for UW2556, UW2557 and UW2558 are statistically identical, indicating that the homogeneous sand at the base of the excavation was deposited rapidly.

An example of the nature of the D_E distribution can be seen in Figure 3, the radial plot for UW2558. Radial graphs plot precision on the x-axis against a standardised value (the number of standard deviations any point is away from some reference) of D_E on the y-axis. The UW2558 graph shows the reference, the central age (similar to the second component), the first component and the third component. The shaded area around the central age represents a two standard deviation envelope so all points falling within it are within two standard deviations of the central age. A line drawn from the origin through any point intersects the right-hand axis at the non-standardised value. The graphs for the three samples showed uniform scatter around the central age, with no indication of separate modes.

This was not the case for the highly dispersed UW2555, which showed at least two modes. The lowest mode consists of low value, low precision grains that form the

first component. More than half the grains (86) yielded negative D_E values, a statistical artefact of modern grains. The central age represents the average of these modern grains and the two older modes, and accounts for very few grains on its own. The third component of UW2555 has a D_E value close to that of the central age of the other three samples and derives from the underlying homogeneous sand, just as some of the upper sands found their way into UW2556. That left the second component as the only mode not derived from somewhere else. Although it represents only 11.4% of the grains, it may provide the age of a real population in the sample.

OSL Ages

Table 2 gives the derived ages based on the central age model for the bottom three samples and a component of UW2555. The ages for the bottom three samples (12.1 ± 1.28 , 13.9 ± 1.59 and 12.8 ± 1.40 ka) are statistically indistinguishable. These three ages indicate that the homogenous sand below the visible bedding is a slightly bioturbated deposit that formed during the Late Pleistocene.

The UW2555 sample is mainly modern sand, as indicated by predominantly zero age values but it contains older grains with a wide variety of ages. The second component with an age of about 5 ka may represent a sand layer deposited at that time, or it may reflect admixing of older sand into an effectively modern deposit.

Discussion

The best interpretation of sample UW2555 is that it is mostly modern, and the small older populations in that sample are the result of bioturbation. This conclusion is based on the proportions of grains in the various populations.

As it is reasonable to take the proportions of single grains in each population as representing the relative proportions of the full sediment body in each age category, the majority of that upper sand unit is not severely bioturbated. This is consistent with the strong field evidence - fine laminations remain which cannot survive mass turnover of the unit. The older populations of grains in this sample (possibly including one with an age of about 5 ka) are the result of bioturbation at the base of the unit, introducing material from the underlying unit. The grains in the top portion of that underlying unit will themselves have undergone bioturbation before the modern sand arrived to cap them, so the upper portion should also show some ages as near-modern, with others indicating the true deposition age.

The four dates reveal a disconformity between the two sand units. The youngest age on the lower unit is 12.1 ka and the upper unit is modern, albeit with grains that might indicate some deposition at about 5 ka, but should probably be interpreted to mean there was

no identifiable deposition at this location during the Holocene. The cause of the commencement of modern sedimentation has been described in detail by Badman (1999) - heavy stocking of cattle and the spread of feral animals, especially rabbits, led to widespread surface erosion and sand mobilisation in the Lake Eyre South catchment between the 1870s and the 1940s. The upper bedded aeolian sand more than 500 mm deep, trapped by vegetation on the rims of dune blowouts, is a result of that sand mobilisation following the arrival of European pastoralists in the 1870s.

Artefacts were recovered from the sediment immediately overlying the surface buried by the UW2555 sample, demonstrating that they were deposited during the Holocene, and possibly within the last 5,000 years. Such an age is consistent with the majority of dates for human occupation of sand deserts elsewhere in Australia, where evidence has suggested a substantial expansion of human activity in the last few millennia (Smith 1993, 2006; Veth 1989; Veth et al. 2001). A set of dates from a single blowout on a single dune however is insufficient to draw conclusions beyond the local level. Further dates from Olympic Dam in deeper stratigraphic contexts will provide information on the recent evolution of the sand dunes and the timing of human occupation in this part of the Australian desert.

Numerous knapping floors on quartzite, silcretes and cherts were identified in the blowout during the investigations, suggesting the stone knappers had been sitting in it, as it is unlikely the tightly clustered features could have been let down in that form by deflation. Less activity took place on the blowout rim as artefact densities, which were 20 and 27 artefacts/m² on average in the blowout, diminished on the margins. In the northern excavated trench (Figure 2) densities decreased away from the blowout floor from 23 to 8/m². The trend was more obvious in the southern trench where artefact densities fell over 6 m from 23/m² near the blowout floor to 5/m² on the rim. Windblown sand has buried artefacts on the rim of the depression indicating that apart from recent sand deposition at its margins, the form of the blowout has changed little since it was occupied.

Acknowledgments

The UW students thank Aaron Nauman for assistance in the UW OSL laboratory, Thanks to BHP Billiton for their support of the UW Australian Desert Archaeology Field School in 2010, and to Peter Hiscock from the Australian National University and Nigel Spooner from the Luminescence Unit at Adelaide University for helpful discussions.

References

- Adamiec, G., and Aitken, M.J. 1998. Dose rate conversion factors: update. *Ancient TL* 16:37-50.
- Aitken, M.J. 1985. *Thermoluminescence Dating*, Academic Press, London.
- Aitken, M.J. 1998. *An Introduction to Optical Dating*. Oxford University Press, London.

- Badman, J.J. 1999. In W. J. H. Slaytor (ed.) Lake Eyre South monograph series volume 6: Archaeology of the Lake Eyre South region. Royal Geographic Society of South Australia
- Bøtter-Jensen, L, and Mejdahl, V. 1988. Assessment of beta dose-rate using a GM multi-counter system. *Nuclear Tracks and Radiation Measurements* 14:187-191.
- Cupper, M.L. 2005. Last glacial to Holocene evolution of semi-arid rangelands in southeastern Australia. *The Holocene* 15(4):541-553.
- Field, T., Marwick, B., Feathers, J. and Przystupa, P. 2011. Four luminescence dates from quartz sand excavated from archaeological site ODO3A23, arid northeastern South Australia. Unpublished report to HEH P/L through Department of Anthropology, University of Washington. June 2011.
- Fitzsimmons, K.E., Rhodes, E.J., Magee, J.W. and Barrows, T.T. 2007. The timing of linear dune activity in the Strzelecki and Tirari Deserts, Australia. *Quaternary Science Reviews*, 26(19-21): 2598-2616.
- Galbraith, R.F., Roberts, R.G., Laslett, G.M., Yoshida, H., & Olley, J.M. 1999. Optical dating of single and multiple grains of quartz from Jimmim rock shelter, northern Australia: Part I, experimental design and statistical models. *Archaeometry* 41:339-364.
- Hesse, P.P., Magee, J.W. and van der Kaars, S. 2004. Late Quaternary climates of the Australian arid zone: a review. *Quaternary International* 118-119:87-102.
- Hollands, C., Nanson, G.C., Jones, B.G., Bristow, C.S., Price, D.M. and Pietsch, T.J. 2006. Aeolian-fluvial interaction: evidence for Late Quaternary channel change and wind-rift linear dune formation in the northwestern Simpson Desert, Australia. *Quaternary Science Reviews* 25:142-6
- Hughes, P.J. and Hiscock, P. 2005: The archaeology of the Lake Eyre South area. In W. J. H. Slaytor (ed.) *Lake Eyre South monograph series volume 6: Archaeology of the Lake Eyre South region*. Royal Geographic Society of South Australia, 1-20.
- Hughes P., Hiscock, P., Sullivan, M. and Marwick, B. 2011. Archaeological investigations at Olympic Dam in arid northeast South Australia. *Journal of the Anthropological Society of South Australia Special Edition Issues in South Australian Aboriginal Archaeology* 34:21-37.
- Jacobs, Z., Duller, G.A.T. and Wintle, A.G. 2006. Interpretation of single grain De distributions and calculation of De. *Radiation Measurements* 41:264-277.
- Lomax, J., Hilgers, A., Twidale, C.R., Bourne J.A. and Radtke, U. 2007. Treatment of broad palaeodose distributions in OSL dating of dune sands from the western Murray Basin, South Australia. *Quaternary Geochronology* 2(1-4):51-56.
- Mabbutt, J.A. 1977. *Desert Landforms*. Australian National University Press, Canberra, 340p.
- Magee, J.W., Miller, G.H., Spooner, N.A., and Questiaux, D. 2004. Continuous 150000 yr monsoon record from Lake Eyre, Australia: Insolation-forcing implications and unexpected Holocene failure. *Geology*, 32(10):885.
- Mayya, Y.S., Morthekai, P., Murari, M.K. and Singhvi, A.K. 2006. Towards quantifying beta microdosimetric effects in single-grain quartz dose distribution. *Radiation Measurements* 41:1032-1039.
- Mitchell, S. 2005. Archaeological Excavations at Olympic Dam, South Australia. In W.J.H. Slaytor (ed.) *Lake Eyre South monograph series volume 6: Archaeology of the Lake Eyre South region*. Royal Geographic Society of South Australia, 21-72.
- Murray-Wallace, C.V., Banerjee, D.B., Bourman, R.P., Olley, J.M. and Brooke, B.P. 2002. Optically stimulated luminescence dating of Holocene relict foredunes, Guichen Bay, South Australia. *Quaternary Science Reviews* 21(8-9):1077-1086.
- Murray, A.S., and Wintle, A.G. 2000. Luminescence dating of quartz using an improved single-aliquot regenerative-dose protocol. *Radiation Measurements* 32:57-73.
- Nanson, G.C., Chen, X.Y. and Price, D.M. 1992. Lateral migration, thermoluminescence chronology and colour variation of longitudinal dunes near Birdsville in the Simpson Desert, central Australia. *Earth Surface Processes and Landforms* 17(8) 807-819.
- Nanson, G.C., Chen, X.Y. and Price, D.M. 1995. Aeolian and fluvial evidence of changing climate and wind patterns during the past 100 ka in the western Simpson Desert, Australia. *Palaeogeography, Palaeoclimatology, Palaeoecology* 113:87-102.
- Olley, J.M., Pietsch, T., & Roberts, R.G. 2004. Optical dating of Holocene sediments from a variety of geomorphic settings using single grains of quartz. *Geomorphology* 60:337-358.
- Prescott, J.R., and Hutton, J.T. 1995. Environmental dose rates and radioactive disequilibrium from some Australian luminescence dating sites. *Quaternary Science Reviews* 14, 439-448.
- Rhodes, E.J. 2011. Optically stimulated luminescence dating of sediments over the past 200,000 years. *Annual Review of Earth and Planetary Sciences* 39(1)461-488.
- Smith, M.A. 1993. Biogeography, human ecology and prehistory in the sandridge deserts. *Australian Archaeology* 37: 35-50.
- Smith, M.A. 2006. Characterizing Late Pleistocene and Holocene stone artefact assemblages from Puritjarra rock shelter: A long sequence from the Australian Desert. *Records of the Australian Museum* 58: 371-410.
- Twidale, C.R., Prescott, J.R., Bourne, J.A. and Williams, F.M. 2001. Age of desert dunes near Birdsville, southwest Queensland. *Quaternary Science Reviews* 20:1355-64.
- Veth, P. 1989. Islands in the interior: a model for the colonization of Australia's arid zone. *Archaeology in Oceania* 24: 81-92.
- Veth, P., Smith, M. and Haley, M. 2001. Kaalpi, the archaeology of an outlying range in the dunefields of the Western Desert. *Australian Archaeology* 52: 9-17.
- Wintle, A.G., 2008. Fifty years of luminescence dating. *Archaeometry* 50:276-312.
- Wintle, A.G. and Murray, A.S., 2006. A review of quartz optically stimulated luminescence characteristics and their relevance in single-aliquot regeneration dating protocols. *Radiation Measurements* 41:369-391.